JCI The Journal of Clinical Investigation

Noncleavable poly(ADP-ribose) polymerase-1 regulates the inflammation response in mice

Virginie Pétrilli, … , Salvatore Cuzzocrea, Zhao-Qi Wang

J Clin Invest. 2004;114(8):1072-1081. https://doi.org/10.1172/JCI21854.

Article **Genetics**

Poly(ADP-ribosyl)ation is rapidly formed in cells following DNA damage and is regulated by poly(ADP-ribose) polymerase-1 (PARP-1). PARP-1 is known to be involved in various cellular processes, such as DNA repair, genomic stability, transcription, and cell death. During apoptosis, PARP-1 is cleaved by caspases to generate 89-kDa and 24-kDa fragments, a hallmark of apoptosis. This cleavage is thought to be a regulatory event for cellular death. In order to understand the biological significance of PARP-1 cleavage, we generated a PARP-1 knockin (*PARP-1*$^{KI/KI}$) mouse model, in which the caspase cleavage site of PARP-1, $DEVD_{214}$, was mutated to render the protein resistant to caspases during apoptosis. While *PARP-1*$^{KI/KI}$ mice developed normally, they were highly resistant to endotoxic shock and to intestinal and renal ischemia-reperfusions, which were associated with reduced inflammatory responses in the target tissues and cells due to the compromised production of specific inflammatory mediators. Despite normal binding of NF-κB to DNA, NF-κB–mediated transcription activity was impaired in the presence of caspase-resistant PARP-1. This study provides a novel insight into the function of PARP-1 in inflammation and ischemia-related pathophysiologies.

Noncleavable poly(ADP-ribose) polymerase-1 regulates the inflammation response in mice

Virginie Pétrilli,[1] Zdenko Herceg,[1] Paul O. Hassa,[2] Nimesh S.A. Patel,[3] Rosanna Di Paola,[4] Ulrich Cortes,[1] Laura Dugo,[4] Helder-Mota Filipe,[5] Christoph Thiemermann,[3] Michael O. Hottiger,[2] Salvatore Cuzzocrea,[4] and Zhao-Qi Wang[1]

[1]International Agency for Research on Cancer (IARC), Lyons, France. [2]Institute of Veterinary Biochemistry and Molecular Biology, University of Zurich, Zurich, Switzerland. [3]William Harvey Research Institute, Queen Mary-University of London, London, United Kingdom. [4]Istituto di Farmacologia, Facoltà di Medicina e Chirurgia, Università di Messina, Torre Biologica Policlinico Universitario, Messina, Italy. [5]Unit of Pharmacology and Pharmacotoxicology, University of Lisbon, Lisbon, Portugal.

Poly(ADP-ribosyl)ation is rapidly formed in cells following DNA damage and is regulated by poly(ADP-ribose) polymerase-1 (PARP-1). PARP-1 is known to be involved in various cellular processes, such as DNA repair, genomic stability, transcription, and cell death. During apoptosis, PARP-1 is cleaved by caspases to generate 89-kDa and 24-kDa fragments, a hallmark of apoptosis. This cleavage is thought to be a regulatory event for cellular death. In order to understand the biological significance of PARP-1 cleavage, we generated a PARP-1 knockin (*PARP-1*$^{KI/KI}$) mouse model, in which the caspase cleavage site of PARP-1, $DEVD_{214}$, was mutated to render the protein resistant to caspases during apoptosis. While *PARP-1*$^{KI/KI}$ mice developed normally, they were highly resistant to endotoxic shock and to intestinal and renal ischemia-reperfusions, which were associated with reduced inflammatory responses in the target tissues and cells due to the compromised production of specific inflammatory mediators. Despite normal binding of NF-κB to DNA, NF-κB–mediated transcription activity was impaired in the presence of caspase-resistant PARP-1. This study provides a novel insight into the function of PARP-1 in inflammation and ischemia-related pathophysiologies.

Introduction

Upon DNA damage, poly(ADP-ribose) polymerase-1 (PARP-1, EC 2.4.2.30) is activated and catalyzes the formation of poly(ADP-ribose) (PAR) chains by transferring (ADP-ribose) from β-NAD^+ onto itself and nuclear acceptor proteins (1). PARP-1 is known to be involved in various cellular processes including DNA repair, recombination, genomic stability, transcription regulation, and cell death (1–3). In addition, massive poly(ADP-ribosyl)ation induced by acute DNA damage results in rapid depletion of cellular NAD^+ and ATP pools, which, if not regulated, can lead to cellular dysfunction and cell death (4). Involvement of PARP-1 in cell death is also speculated based on the prominent phenomenon that during apoptosis, PARP-1 is cleaved by caspases at the conserved site $DEVD_{214}$, generating 24-kDa and 89-kDa fragments, a hallmark of apoptosis.

Mice lacking PARP-1 develop normally and *PARP-1*$^{-/-}$ fibroblasts and lymphoid cells display a normal apoptotic response after treatment with various apoptotic inducers, such as anti-Fas antibody, TNF-α, γ-radiation, and dexamethasone, which demonstrates that PARP-1 per se is dispensable for apoptosis, at least in these cell types (5, 6). However, inactivation of PARP-1 by chemical inhibitors and genetic means protects mice from endotoxic shock and other disease models related to inflammation, such as diabetes, stroke, and myocardial reperfusion (7–12). In addition, PARP inhibitors protect rats from renal and intestinal ischemia-reperfusion–induced (I/R-induced) lethality and tissue injury (13, 14). The mechanism underlying these models is believed to involve massive PARP-1 activation induced by oxidative DNA damage, resulting in tissue injury via depletion of cellular pools of NAD^+/ATP, which causes cell death (4, 10).

Sepsis is a systemic inflammatory response syndrome to localized or systemic infections that causes the overproduction of proinflammatory cytokines, such as TNF-α and IL-1β, and ultimately results in multiple organ failure (15). LPS, an endotoxin found in the outer membrane of Gram-negative bacteria, is a major trigger of sepsis. Endotoxic shock has been used to test the inflammation response in animal models. *PARP-1*$^{-/-}$ mice are highly resistant to LPS (9, 16). The increased survival of such mice compared with wild-type is associated with a low TNF-α and NO production, which is believed to be due to the impaired transcriptional activity of NF-κB in the absence of PARP-1 (3, 9, 17, 18). While some in vitro studies have demonstrated an involvement of poly(ADP-ribosyl)ation in the DNA binding activity of NF-κB (19, 20), others have shown that PARP-1 activity is dispensable for this transcription regulation process (17). Taken together, these studies indicate a role for PARP-1 in inflammation response.

Although cleavage of PARP-1 by caspases at the DEVD site is a universal phenomenon during apoptosis, the significance of this cleavage in vivo is largely unknown. It is postulated that PARP-1 cleavage might occur in cells undergoing apoptosis to inactivate their capacity to repair DNA in order to preserve energy pools (21, 22). It is also proposed that the 24-kDa product of PARP-1 cleavage irreversibly binds to DNA in order to prevent the access of DNA repair enzymes to fragmented DNA (23, 24). Consistent with these hypotheses, cell lines expressing a caspase-resistant PARP-1 by mutating the $DEVD_{214}$ site displayed increased apoptosis and necrosis after TNF-α treatment (25–27). These studies indicate that the caspase cleavage of PARP-1 is an important regulatory event in cellular functions.

Nonstandard abbreviations used: AST, aspartate aminotransferase; EMSA, electromobility shift assay; I/R, ischemia-reperfusion; KI, knockin; MDA, malondialdehyde; MEF, mouse embryonic fibroblast; MLF, mouse lung fibroblast; MPO, myeloperoxidase; NOS-2, NO synthase-2; PAR, poly(ADP-ribose); PARP-1, poly(ADP-ribose) polymerase-1; SAO, splanchnic artery occlusion; Z-VAD-fmk, *N*-benzyloxycarbonyl-Val-Ala-Asp-fluoromethyl ketone.

Conflict of interest: The authors have declared that no conflict of interest exists.

Citation for this article: *J. Clin. Invest.* **114**:1072–1081 (2004). doi:10.1172/JCI200421854.

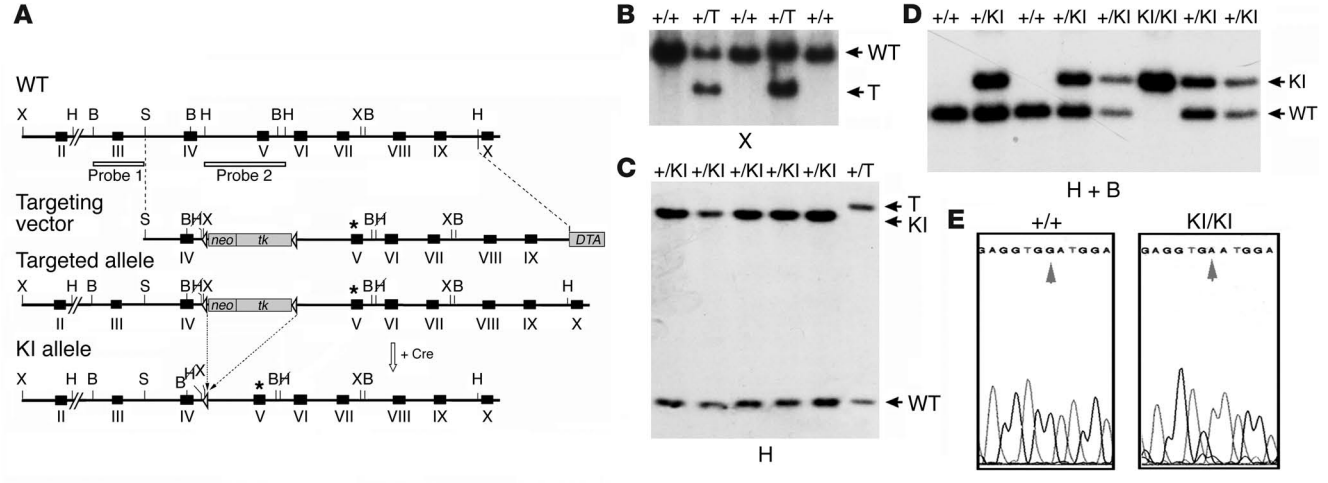

Figure 1
Generation of *PARP-1*$^{KI/KI}$ mice. (**A**) Structure of the targeting vector and partial restriction map of the *PARP-1* locus before and after homologous recombination and Cre-mediated recombination. Exons are indicated by black boxes, and positions of two Southern blot probes are represented by open boxes. Targeted allele and KI allele of *PARP-1* after gene targeting and Cre-mediated recombination, respectively, are shown. Lox-P sites are represented by open triangles. The point mutation (D214N) is indicated by an asterisk. Restriction enzymes: *Hin*dIII (H); *Bam*HI (B); *Xho*I (X); *Sal*I (S). Crossed letter H represents the *Hin*dIII site that is abolished during cloning of a targeting vector. (**B** and **C**) Southern blot analysis of *PARP-1*–targeted (+/T) (**B**) and *PARP-1*$^{+/KI}$ (+/KI) (**C**) ES cell DNA after digestion with *Xho*I and *Hin*dIII, respectively, and hybridization with probe 1 (**B**) and probe 2 (**C**). Cre-mediated recombination causes a deletion of the *neo*/*tk* cassette resulting in a size reduction after *Hin*dIII digestion. The genotype of individual ES clones is indicated above of the gels. (**D**) Genotyping of offspring from intercrosses of *PARP-1*$^{+/KI}$ heterozygous mice by Southern blotting using probe 2. The genotype of individual animals is indicated above the blot. (**E**) Results of sequencing of DNA obtained from a wild-type (*PARP-1*$^{+/+}$; +/+) and a *PARP-1*$^{KI/KI}$ (KI/KI) mouse. Arrows indicate the presence of G → A transition at codon 214 in the *PARP-1*$^{KI/KI}$ mouse.

To investigate the physiological relevance of PARP-1 cleavage in cell death and inflammation, we engineered a mutant mouse strain by introducing a point mutation into the caspase cleavage site of the *PARP-1* gene by a "knockin" (KI) strategy. Although PARP-1 knockin (*PARP-1*$^{KI/KI}$) mice developed normally, they were resistant to intestinal and renal I/R and endotoxic shock models due to a downregulation of NF-κB transcriptional activity and inflammation mediators.

Results

PARP-1$^{KI/KI}$ *mice develop normally*. The conversion of aspartate to asparagine at the 214 codon (Asp214Asn; D214N) renders the PARP-1 protein resistant to caspase cleavage (25). We constructed the targeting vector containing such a point mutation (D214N) at exon 5 of the *PARP-1* gene introduced by a site-directed mutagenesis (Figure 1A). After electroporation of the targeting vector into ES cells and homologous recombination, ES clones containing a targeted allele (*PARP-1*$^{+/T}$) were identified by Southern blot analysis (Figure 1B). To avoid interference of the selection cassette in the intronic sequence, we removed the cassette expressing the *neomycin resistance* gene (*neo*) and the *thymidine kinase* gene (*tk*) by transient expression of the Cre recombinase in targeted heterozygous ES cells, generating a knockin allele in ES cells (*PARP-1*$^{+/KI}$) (Figure 1, A and C). *PARP-1*$^{+/KI}$ ES cells were used to generate heterozygous *PARP-1*$^{+/KI}$ animals. After these *PARP-1*$^{+/KI}$ mice were intercrossed, *PARP-1*$^{KI/KI}$ mice were obtained at a Mendelian ratio and exhibited no apparent developmental abnormalities compared with wild-type littermates (data not shown). The presence of the introduced mutation in *PARP-1*$^{KI/KI}$ mice was confirmed by sequencing the locus (Figure 1E).

Characterization of caspase-resistant PARP-1. We first examined by Western blotting expression levels of the mutant PARP-1 protein in *PARP-1*$^{KI/KI}$ mice and found an equal amount of the protein expressed in *PARP-1*$^{KI/KI}$ and wild-type fibroblasts, thymocytes, and macrophages, which were the cell types used in the present study (data not shown). To confirm that the point mutation introduced at the DEVD site renders PARP-1 resistant to caspase cleavage, we activated caspases in thymocytes, a cell type that undergoes classic apoptosis, after dexamethasone treatment. Western blot analysis revealed that 9 hours after dexamethasone treatment, significant cleavage of PARP-1 was observed in wild-type extracts as shown by the presence of the 89-kDa band, whereas extracts from *PARP-1*$^{KI/KI}$ thymocytes presented only 1 band at 113 kDa corresponding to the full length of PARP-1 (Figure 2A). To rule out the possibility that mutant PARP-1 could act as a competitive inhibitor of caspases, we measured at different time points caspase-3 activity in these cell extracts after dexamethasone treatment. As shown in Figure 2B, the kinetics of induction and activity of caspase-3 were similar in wild-type and *PARP-1*$^{KI/KI}$ cells with a peak at 6 hours, which indicated that caspase-resistant PARP-1 had no inhibitory effect on caspase-3 activity. Thus, mutant PARP-1 is effectively resistant to caspase cleavage during apoptosis in thymocytes and does not interfere with caspase-3 activity.

To investigate whether the point mutation introduced would affect the PARP-1 catalytic activity, we used a biochemical assay to test the PAR polymerase activity of noncleavable PARP-1 in vitro by measuring auto-poly(ADP-ribosyl)ation of PARP-1, since it is the major target of this modification. Figure 2C shows that cellular extracts from wild-type and *PARP-1*$^{KI/KI}$ primary mouse embryonic fibroblasts (MEFs) exhibited a similar amount of the PARP-1 protein and a similar extent of PAR synthesis at the size of 113 kDa, which corresponds to PARP-1. To examine whether mutant PARP-1 was functional in vivo, we induced DNA damage in MEFs using

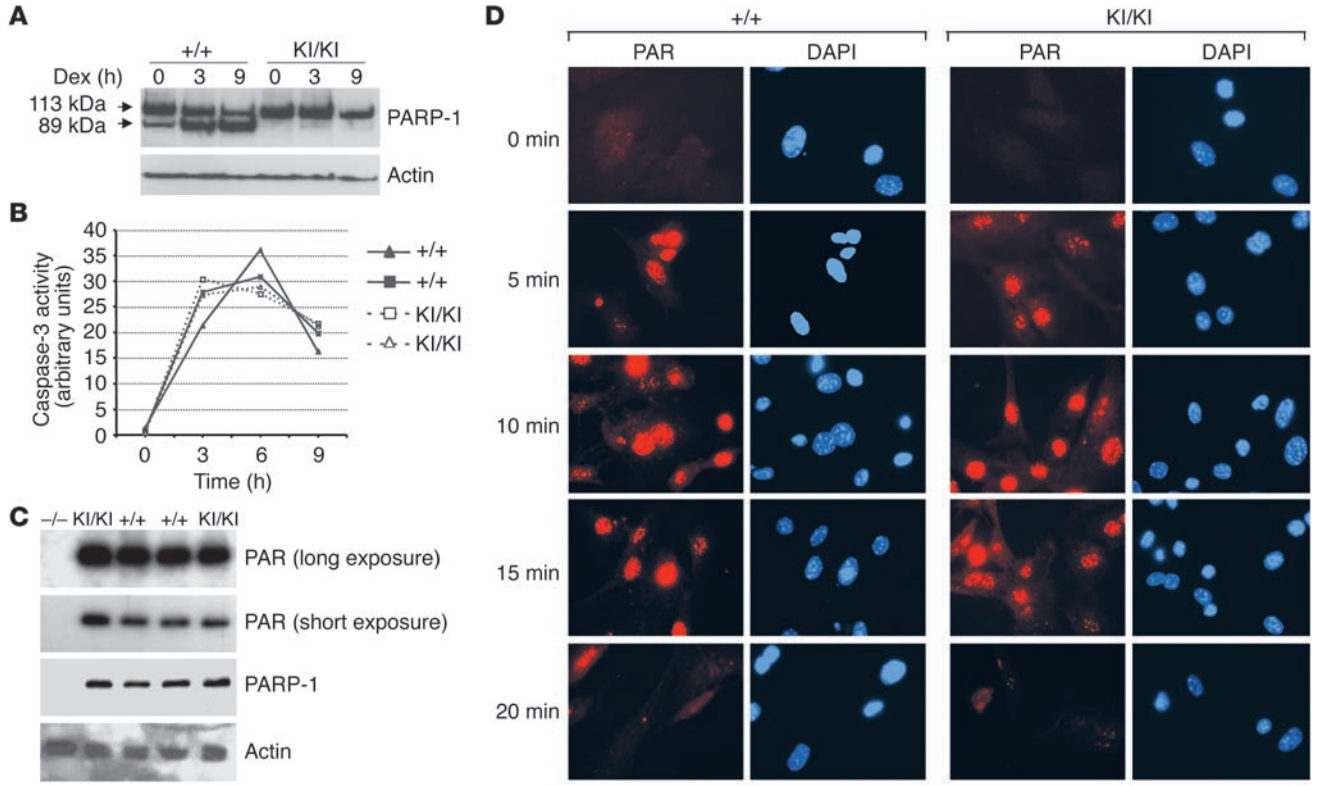

Figure 2
Characterization of mutant PARP-1. (**A**) Western blot analysis showing the cleavage of PARP-1 in cell extracts from *PARP-1*$^{+/+}$ and *PARP-1*$^{KI/KI}$ thymocytes treated with 1 μM dexamethasone (Dex) for 3 and 9 hours. Note intact PARP-1 in *PARP-1*$^{KI/KI}$ cell extracts. Actin was used as a loading control. This experiment was repeated at least 2 times. (**B**) Caspase-3 activity was measured using 2 sets of *PARP-1*$^{+/+}$ and *PARP-1*$^{KI/KI}$ thymocytes after treatment with 1 μM dexamethasone for 3, 6, and 9 hours. (**C**) Enzymatic activity analysis in *PARP-1*$^{KI/KI}$ MEFs. Cell extracts from indicated genotypes were prepared and the polymer (PAR) formation was visualized by incubating the blot with ^{32}P-labeled NAD$^+$. The blot was re-hybridized with anti–PARP-1 and anti-actin antibodies. *PARP-1*$^{-/-}$ (–/–) MEFs were used as a control. This experiment was repeated at least 2 times. (**D**) Immunofluorescence staining of polymers (PAR). MEFs were incubated with 200 μM H_2O_2, fixed at the indicated time points, and labeled with the anti-PAR antibody (red). Nuclei were stained with DAPI (blue).

H_2O_2 and stained the cells using an antibody directed against PAR. Staining of polymers revealed that *PARP-1*$^{KI/KI}$ MEFs displayed the same level and kinetics of formation as wild-type cells after H_2O_2 treatment (Figure 2D). Specifically, PAR formed after 5 minutes, reached peaks at 10 minutes, and decreased after 20 minutes (Figure 2D). Taken together, these results demonstrate that the point mutation introduced at the DEVD site did not affect the protein expression and PARP-1 activity in response to DNA damage.

PARP-1$^{KI/KI}$ *mice are resistant to endotoxic shock.* In order to test whether PARP-1 cleavage is involved in the response to LPS-induced septic shock, we treated mice of both *PARP-1*$^{+/+}$ and *PARP-1*$^{KI/KI}$ genotypes with LPS and monitored survival over a period of 7 days. Interestingly, *PARP-1*$^{KI/KI}$ mice were more resistant to LPS treatment compared with wild-type mice, as approximately 40% of *PARP-1*$^{KI/KI}$ mice survived, whereas all wild-type counterparts died ($P = 0.0463$; Figure 3A). In order to examine the nature of the reduced inflammatory response, we measured proinflammatory cytokines released in the blood of wild-type and *PARP-1*$^{KI/KI}$ mice 2 hours after LPS treatment. As shown in Figure 3B, the induction of IL-1β was significantly compromised ($P = 0.03$) in *PARP-1*$^{KI/KI}$ sera compared with that of wild-type mice. Similarly, the production of TNF-α was also lower in *PARP-1*$^{KI/KI}$ sera compared with that of wild-type counterparts, although the difference was not statistically significant (Figure 3C). These results suggest that noncleavable PARP-1 compromises an inflammatory response induced by LPS.

Impaired induction of NO synthase-2 in PARP-1$^{KI/KI}$ *macrophages.* To examine the status of NO production, we isolated peritoneal macrophages from wild-type and *PARP-1*$^{KI/KI}$ mice and stimulated them in culture dishes with LPS. After 24 hours, supernatant was collected and nitrite was measured. Figure 4A shows that *PARP-1*$^{KI/KI}$ macrophages secreted about 50% less NO than the wild-type counterparts. As a control, *PARP-1*$^{-/-}$ macrophages also secreted less NO (data not shown), consistent with a previous study (9). Because iNOS/NO synthase-2 (iNOS/NOS-2) is responsible for the production of NO by macrophages, we analyzed NOS-2 expression in *PARP-1*$^{KI/KI}$ macrophages. Western blot analysis revealed that the expression of NOS-2 was greatly reduced compared with wild-type cells (Figure 4B), which correlated with the reduced synthesis of NO by *PARP-1*$^{KI/KI}$ macrophages. Northern blot analysis further confirmed that the downregulation of NOS-2 was due to dramatically reduced transcription of the *nos-2* gene in *PARP-1*$^{KI/KI}$ macrophages (Figure 4C). Thus, the response of *PARP-1*$^{KI/KI}$ macrophages to LPS is compromised most likely due to misregulation of inflammation mediators.

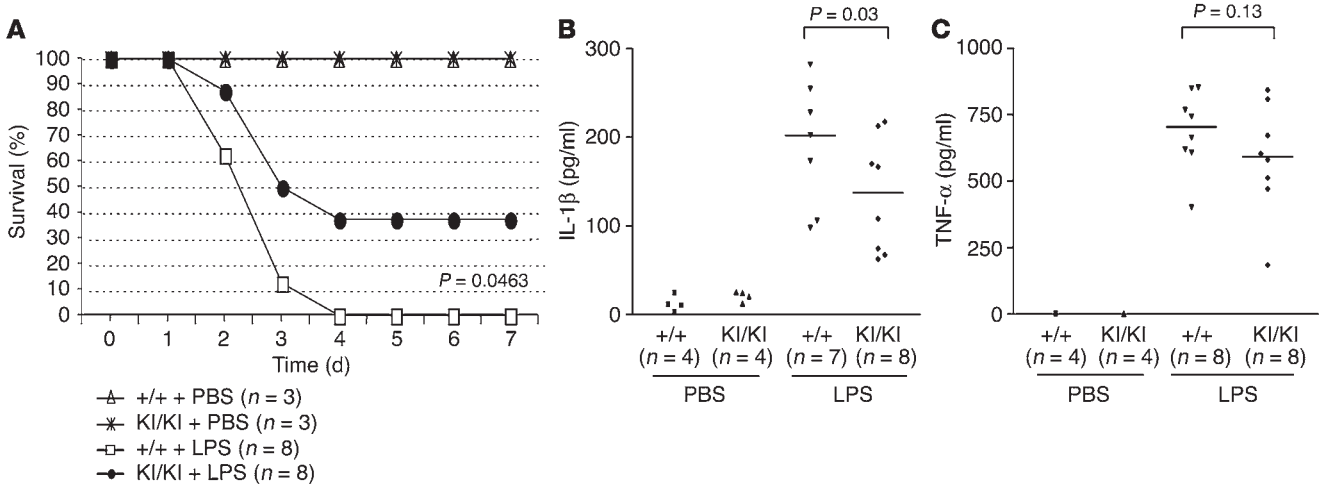

Figure 3
PARP-1$^{KI/KI}$ mice are resistant to endotoxic shock. (**A**) *PARP-1*$^{+/+}$ and *PARP-1*$^{KI/KI}$ mice were treated with LPS or PBS, and their survival was monitored over 7 days. A representative experiment is shown with indicated numbers of mice (*n*) in each group. The experiment was repeated at least 3 times. (**B** and **C**) Levels of IL-1β (**B**) and TNF-α (**C**) in mouse sera 2 hours after LPS or PBS treatment were analyzed by ELISA. Number of mice with each measurement is indicated. Data in **B** and **C** represent 1 of 2 independent experiments.

Noncleavable PARP-1 regulates the activity of NF-κB. To investigate whether *nos-2* downregulation was due to impaired NF-κB activity, we next analyzed the NF-κB function in *PARP-1*$^{KI/KI}$ cells in response to LPS (9, 17). To test the binding activity of NF-κB to DNA, we incubated nuclear extracts of macrophages stimulated with LPS using a probe containing the NF-κB consensus sequence. Electromobility shift assay (EMSA) analysis revealed that NF-κB bound to the κB sequences in *PARP-1*$^{KI/KI}$ nuclear extracts as efficiently as in wild-type extracts (Figure 5A). The specificity of the binding was assessed by incubating the extracts with a cold probe and also a probe containing a mutation in the NF-κB consensus sequence (data not shown).

To test NF-κB transcriptional activity in the presence of caspase-resistant PARP-1, we transfected an NF-κB reporter vector containing the *nos-2* promoter into *PARP-1*$^{+/+}$ or *PARP-1*$^{KI/KI}$ mouse lung fibroblasts (MLFs) and found that NF-κB transcriptional activity was severely impaired in *PARP-1*$^{KI/KI}$ cells in response to LPS or LPS plus IFN-γ treatment (Figure 5B). The same transfection experiments with a reporter gene under the control of mutated κB sites demonstrated that the observed induction was NF-κB specific. We next performed reconstitution experiments to examine the function of wild-type, noncleavable, and enzyme-dead PARP-1 in the NF-κB–mediated transactivation of target genes in response to LPS and IFN-γ. To this end, we cotransfected *PARP-1*$^{-/-}$ macrophages, which are defective in NF-κB transactivation, with an NF-κB reporter together with a vector expressing either a wild-type, a caspase-resistant PARP-1 (D214N), or an enzyme-dead PARP-1 (M890V/D899N) (Figure 5C). Similar expression levels of these vectors in these cells were detected by Western blotting (Figure 5D). NF-κB transcriptional activity was not restored in *PARP-1*$^{-/-}$ macrophages reconstituted with noncleavable PARP-1 (D214N) compared with those reconstituted with a wild-type PARP-1 (Figure 5C, upper panel). Interestingly, an enzyme-dead PARP-1 fully restored the NF-κB transcriptional activity in *PARP-1*$^{-/-}$ macrophages to the level of cells reconstituted by wild-type PARP-1 (Figure 5C, lower panel). Thus, NF-κB transcriptional activity is impaired in *PARP-1*$^{KI/KI}$ cells in response to LPS alone or to LPS plus IFN-γ.

These data suggest that PARP-1 cleavage regulates NF-κB functions. We attempted to test whether PARP-1 is indeed cleaved in response to LPS in macrophages. We failed to detect any cleaved products of PARP-1 in primary mouse macrophages upon LPS stimulation (data not shown) because the anti–PARP-1 antibody (C2-10) did not efficiently recognize the cleaved products of PARP-1 in mouse or in human cells. Therefore, we used a human macrophage-like cell line (THP-1) and a newly generated human PARP-1–specific antibody. We

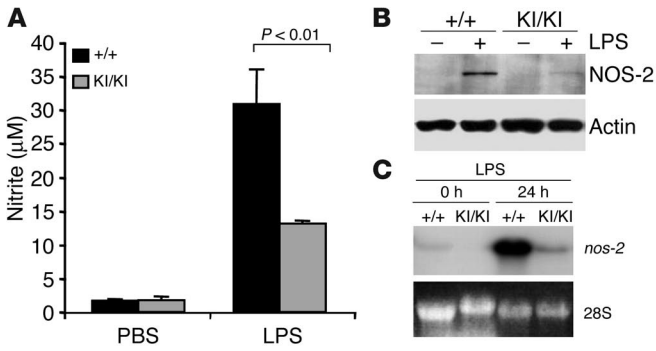

Figure 4
Induction of NO and NOS-2 in *PARP-1*$^{KI/KI}$ macrophages by LPS. (**A**) *PARP-1*$^{+/+}$ and *PARP-1*$^{KI/KI}$ macrophages were treated with LPS (1 μg/ml) for 24 hours, and nitrite in the medium was measured. The data are from pooled macrophages of 4 mice, values are the mean of duplicate measurements, and the study was repeated at least 3 times. (**B**) Western blot analysis of NOS-2 from macrophages treated with or without LPS for 24 hours. Note a great reduction of NOS-2 expression in *PARP-1*$^{KI/KI}$ cells compared with *PARP-1*$^{+/+}$ samples. Actin was used as a loading control. This experiment was repeated three times. (**C**) Northern blot analysis of *nos-2* expression in macrophages treated with LPS for 24 hours. Ethidium bromide staining of 28S rRNA was used as a loading control. Note a significant reduction in *nos-2* expression in *PARP-1*$^{KI/KI}$ macrophages compared with *PARP-1*$^{+/+}$ counterparts. This Northern blot is from 1 of the 2 experiments.

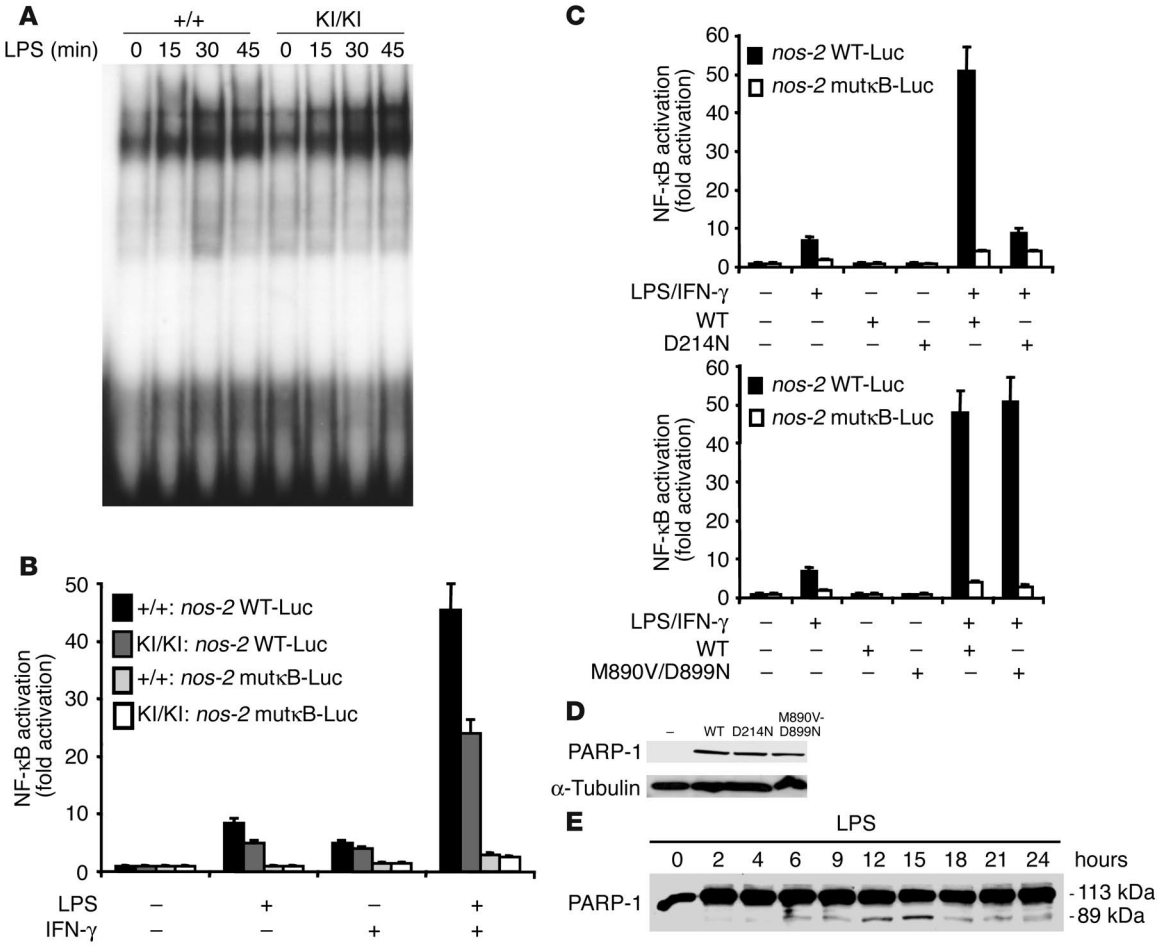

Figure 5

Noncleavable PARP-1 impairs NF-κB–dependent gene expression in response to proinflammatory stimuli. (**A**) EMSA analysis of NF-κB binding activity in *PARP-1*$^{+/+}$ and *PARP-1*$^{KI/KI}$ macrophage extracts. This experiment was repeated at least 5 times using 3 independent sets of samples. (**B**) Primary *PARP-1*$^{+/+}$ MLFs and *PARP-1*$^{KI/KI}$ MLFs were transfected with the indicated luciferase reporter vectors: *nos-2*(1485/+31WT)-Luc (*nos-2* WT-Luc) and *nos-2*(1485/+31NF-κBmut)-Luc (nos-2 mutκB-Luc). The luciferase activity was measured after stimulation by LPS and/or IFN-γ for 12 hours. (**C**) Primary *PARP-1*$^{-/-}$ peritoneal macrophages were cotransfected with *nos-2*(1485/+31WT)-Luc or *nos-2*(1485/+31NF-κBmut)-Luc, together with vectors expressing wild-type PARP-1 (WT) or caspase-resistant PARP-1 (D214N; upper panel) or enzyme-dead PARP-1 (M890V/D899N; lower panel). NF-κB activation (fold increase) in **B** and **C** was determined by the ratio of the luciferase activity between cells treated and untreated with LPS and IFN-γ. The value of untreated cells was arbitrarily set to 1. Error bars indicate standard errors of 3 independent experiments. (**D**) Western blot analysis shows corresponding PARP-1 proteins used in panel **C**. (**E**) Western blot analysis of PARP-1 cleavage in THP-1 cells upon LPS stimulation. Note that PARP-1 cleavage products are readily visible 6 hours after LPS stimulation. This Western blot is representative of the 2 experiments.

found by Western blotting that PARP-1 was cleaved in these cells in response to LPS treatment, albeit in a small amount (Figure 5E).

PARP-1$^{KI/KI}$ *mice are protected from intestinal I/R.* Intestinal I/R induces proinflammatory cascade in the gut, which can culminate in multiple organ dysfunction syndrome (28). We next performed intestinal I/R experiments by splanchnic artery occlusion (SAO). While SAO shock resulted in the death of 50% of *PARP-1*$^{+/+}$ mice at 2 hours after reperfusion, only 30% of *PARP-1*$^{KI/KI}$ mice died after SAO shock. All sham-operated mice survived the entire 2-hour observation period. A histological examination at 60 minutes after reperfusion revealed a disruption of intestinal mucosa and a loss of the villi structure in wild-type ileum sections (Figure 6A). It was also evident that infiltration of neutrophils, lymphocytes, and plasma cells extended through the wall and concentrated below the epithelial layer, with occasional focal ulceration (Figure 6A). In contrast, *PARP-1*$^{KI/KI}$ mice showed a marked reduction in histological alterations, inflammatory cell infiltration, or exudate formation (Figure 6B). No intestinal injury was found in tissue sections from sham-operated mice (Figure 6C). These results suggest that noncleavable PARP-1 protects mice from intestinal injury by I/R.

Inflammation response and oxidative damage are reduced in PARP-1$^{KI/KI}$ *mice.* The release of free radicals and oxidant molecules during the early phase of reperfusion has been suggested to cause tissue necrosis and mucosal dysfunction (29). Intestinal I/R induced a marked increase in tissue-positive staining for nitrotyrosine, a marker of tissue injury, in the epithelium of the small intestine of wild-type mice (Figure 6D). We found very weak staining for nitrotyrosine in the intestine of *PARP-1*$^{KI/KI}$ mice subjected to SAO treatment (Figure 6E). It was also noted that there was no staining for nitrotyrosine in the intestine obtained from sham-operated mice (Figure 6F).

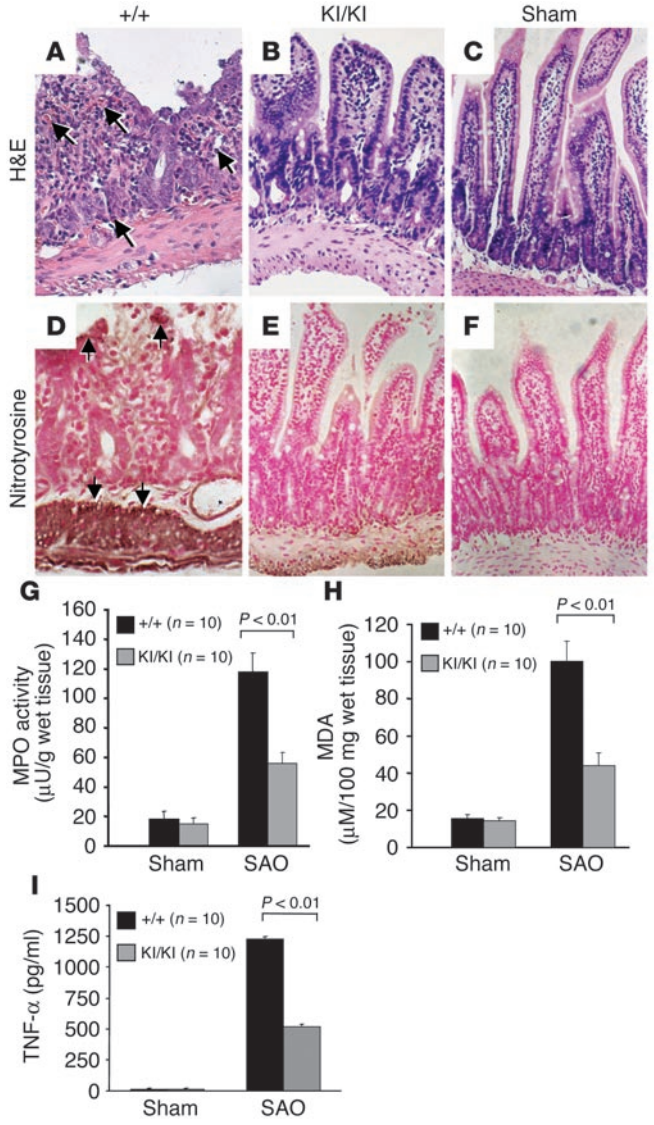

Figure 6
PARP-1$^{KI/KI}$ mice are protected from intestinal I/R injury. (**A**–**C**) H&E staining of ileums. (**A**) The SAO-shocked ileum from a *PARP-1*$^{+/+}$ animal exhibits destroyed villi and mucosa. Infiltration of neutrophils and leukocytes (arrows) is evident. (**B**) The ileum from a *PARP-1*$^{KI/KI}$ mouse showing a relatively normal structure of villi and mucosa. (**C**) The ileum from a sham-operated animal. (**D**–**F**) Nitrotyrosine staining of the ileum after SAO treatment. A strong staining of nitrotyrosine (e.g., arrows in **D**) in the ileum from a *PARP-1*$^{+/+}$ animal is in contrast to the weak staining in the *PARP-1*$^{KI/KI}$ ileum (**E**). (**F**) A weak staining for nitrotyrosine is shown in the sham-operated ileum. (**G**) MPO activity was significantly lower in *PARP-1*$^{KI/KI}$ mice after SAO shock compared with that in *PARP-1*$^{+/+}$ controls. (**H**) After SAO shock, the level of MDA induction was significantly lower in intestines of *PARP-1*$^{KI/KI}$ mice compared with *PARP-1*$^{+/+}$ mice. (**I**) A significant reduction of the increase of TNF-α levels was observed in the plasma from SAO-shocked *PARP-1*$^{KI/KI}$ mice when compared with wild-type mice. Ten mice were used for each treatment. Original magnification (**A**–**F**), ×180. Data in (**G**–**I**) represent the mean ± SEM for 10 observations.

We next examined whether the protection of tissue damage in *PARP-1*$^{KI/KI}$ mice was due to reduced inflammation. Infiltration of inflammatory cells (mainly neutrophils) in the intestine is associated with the induction of myeloperoxidase (MPO) activity. We found that while MPO activity was significantly elevated at 60 minutes after reperfusion in the intestine from SAO-shocked wild-type mice, the induction was significantly reduced ($P < 0.01$) in the SAO-shocked *PARP-1*$^{KI/KI}$ intestine in comparison with that in wild-type mice (Figure 6G). We further assessed the status of peroxidation in the intestine of SAO-shocked mice. While high levels of malondialdehyde (MDA), indicative of lipid peroxidation, were detected in the wild-type intestines 60 minutes after reperfusion, the MDA levels in the *PARP-1*$^{KI/KI}$ intestine were significantly lower than those in wild-type mice ($P < 0.01$) (Figure 6H).

Finally, we evaluated the serum levels of TNF-α at 60 minutes after reperfusion and found that this cytokine was significantly elevated in the plasma from SAO-shocked wild-type mice ($P < 0.01$). However, a significantly reduced TNF-α induction was observed in the plasma from SAO-shocked *PARP-1*$^{KI/KI}$ mice (Figure 6I).

PARP-1$^{KI/KI}$ *mice are protected from renal I/R.* To test the generality of caspase-resistant PARP-1 in protecting mice from inflammation and tissue injury, we examined the response of *PARP-1*$^{KI/KI}$ mice in another I/R pathological model; i.e., renal I/R that causes the injury and death of renal cells leading to renal dysfunction and failure (30–33). I/R caused a significant increase in the plasma levels of urea, creatinine, aspartate aminotransferase (AST), and nitrite/nitrate in wild-type mice compared with sham-operated mice (Figure 7, A–D), which suggests a significant degree of renal dysfunction, reperfusion injury, and NO synthesis. In contrast to wild-type mice, I/R-treated *PARP-1*$^{KI/KI}$ mice showed significantly attenuated renal dysfunction, as measured by plasma urea and creatinine levels (Figure 7, A and B), and reperfusion injury, as measured by plasma AST levels (Figure 7C). In addition, the induction of plasma nitrite/nitrate concentrations was abolished in *PARP-1*$^{KI/KI}$ mice subjected to I/R (Figure 7D). Histological examination of kidneys revealed that wild-type mice subjected to I/R showed a significant degree of renal injury (Figure 7E) when compared with sham-operated wild-type mice (Figure 7G). Specifically, I/R-treated wild-type kidneys exhibited degeneration of tubular structure, tubular dilatation, swelling and necrosis, luminal congestion, and eosinophilia (Figure 7E). In contrast, I/R-treated *PARP-1*$^{KI/KI}$ renal sections showed a marked reduction in the severity of these histological features of renal injury (Figure 7F) when compared with kidneys obtained from wild-type mice subjected to I/R only (Figure 7E).

We next measured the MPO activity in the kidney tissues after I/R and found that it was significantly lower in *PARP-1*$^{KI/KI}$ kidneys compared with those of the wild-type counterparts (Figure 7H). Finally, there was no difference in any of the above biochemical and histological parameters measured between sham-operated *PARP-1*$^{KI/KI}$ mice and sham-operated wild-type controls (see Figure 7, A–D, H). These results demonstrate that *PARP-1*$^{KI/KI}$ mice were resistant to tissue damage caused by renal I/R.

Caspase inhibitor attenuates inflammation in intestinal and renal I/R models. To further evaluate whether PARP-1 cleavage is responsible for the protective effects against I/R treatment, we used a broad caspase inhibitor (*N*-benzyloxycarbonyl-Val-Ala-Asp-fluoromethyl ketone; Z-VAD-fmk) in these models. The administration of Z-VAD-fmk prior to SAO treatment protected the ileum of wild-type mice from tissue injury (Figure 8, A–C). Specifically, the structure of intestinal mucosa and villi was preserved in wild-type mice pre-

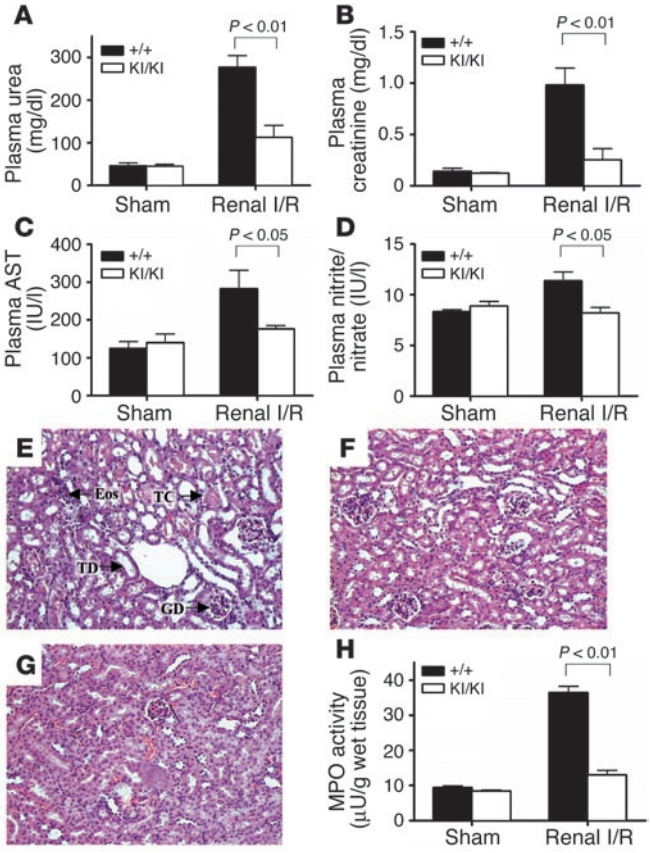

Figure 7

PARP-1$^{KI/KI}$ mice are protected from renal I/R. (**A**–**D**) Biochemical parameters of mice subjected to sham-operation or renal I/R. (**A**) Plasma urea and (**B**) creatinine levels were measured as markers of renal dysfunction. (**C**) Plasma AST levels were measured as a marker of reperfusion injury. (**D**) Plasma nitrite/nitrate levels were measured as a marker of nitric oxide synthesis. (**E**–**G**) Histological analysis (H&E) of renal sections of mice subjected to sham-operation or renal I/R. (**E**) A renal section of a wild-type mouse subjected to renal I/R showing glomerular degeneration (GD), tubular dilatation (TD), tubular congestion (TC), and the presence of eosinophilia (Eos). (**F**) A *PARP-1*$^{KI/KI}$ kidney after renal I/R displayed a reduction in renal injury. (**G**) A section from a sham-operated mouse. Original magnification, ×125. (**H**) Renal MPO activity was measured as a marker of neutrophil infiltration subsequent to sham operation or renal I/R. Wild-type sham: $n = 6$; *PARP-1*$^{KI/KI}$ sham: $n = 4$; wild-type renal I/R: $n = 8$; *PARP-1*$^{KI/KI}$ renal I/R: $n = 8$. Data in **A**–**D** and **H** represent the mean ± SEM for n observations.

treated with the inhibitor, which was in contrast with mice pretreated with the solvent only (vehicle). Consistently, MPO activity in the gut from mice pretreated with Z-VAD-fmk was reduced (Figure 8D). Similarly, the caspase inhibitor also attenuated tissue injury from renal I/R treatment as judged by the reduction of creatinine and urea in the plasma (Figure 8, E and F), although the urea level was not statistically different from that in the vehicle-treated group, which may be attributable to the regime of this specific model in which the reperfusion lasted 24 hours.

Discussion

Once apoptosis is triggered in cells, PARP-1 is cleaved by activated caspases, mainly by caspase 3, but also by caspase 7. In order to investigate the physiological significance of this cleavage, we generated a mouse model designed as *PARP-1* KI (*PARP-1*$^{KI/KI}$) mice. Although these mice do not show apparent spontaneous abnormalities, they are hyperresistant to tissue injuries induced by inflammation and I/R due to the downregulation of NF-κB transcriptional activity, which results in the compromised production of specific inflammatory mediators. These results suggest that the PARP-1 cleavage event is physiologically relevant in the regulation of an inflammatory response in vivo.

We found that *PARP-1*$^{KI/KI}$ mice are protected from LPS-induced endotoxic shock. LPS activates the adaptive immune system by inducing the release of proinflammatory molecules (34). IL-1β, a proinflammatory cytokine, and NO, an antimicrobial cytotoxic agent, are major mediators of the acute inflammatory response to microorganisms (35, 36). Our study shows that the resistance of *PARP-1*$^{KI/KI}$ mice to LPS-induced septic shock is associated with a decreased secretion of IL-1β in blood and a decreased production of NO by macrophages. In local pathophysiological models caused by I/R, we observed that *PARP-1*$^{KI/KI}$ mice were protected from SAO shock–induced inflammation, which correlates with a preserved intestinal villi histology, reduced MPO activity and TNF-α in the blood, as well as low levels of nitrotyrosine and lipid peroxidation in the target tissues. In addition, we found a similar resistance in *PARP-1*$^{KI/KI}$ mice to renal I/R treatment. Biochemical analysis showed that *PARP-1*$^{KI/KI}$ mice are protected from renal failure due to the reduced renal tissue injury (see Figure 7).

It has been hypothesized that the protective function of PARP-1 deficiency against I/R injury and also endotoxic shock may be attributed to the preservation of cellular pools of NAD^+/ATP and consequently reduced cell death (4, 9). However, since in *PARP-1*$^{KI/KI}$ mice, PARP-1 is intact and cannot be cleaved by caspases, the current study suggests that proper proteolysis of the PARP-1 protein is an important regulatory event in cellular functions, particularly in inflammatory response. In fact, the production of proinflammatory mediators, such as NO, was impaired in *PARP-1*$^{KI/KI}$ macrophages. This reduction correlates with the downregulation of *nos-2* gene expression (Figure 4). This observation is consistent with the notion that NOS-2 activity is responsible for the production of nitrotyrosine and lipid peroxidation (29). Thus, the protection of *PARP-1*$^{KI/KI}$ mice from LPS and I/R appears to be due to the impaired induction of NOS-2. It is also interesting to note that *nos-2* deletion and NOS-2 inhibitor protected mice from renal and intestinal I/R treatment due to a diminished nitrotyrosine formation and low MDA levels in target tissues (29, 37).

Thus, PARP-1 cleavage seems to regulate expression of inflammation mediators through its role in coactivation with NF-κB. Indeed, we found that NF-κB transcriptional activity was impaired in *PARP-1*$^{KI/KI}$ cells in response to inflammatory stress. Despite normal capacity of NF-κB binding to consensus sequences, its transcriptional activity was impaired in *PARP-1*$^{KI/KI}$ cells. Interestingly, since PARP-1 was fully enzymatic active in *PARP-1*$^{KI/KI}$ mice and enzyme dead PARP-1 could restore NF-κB activity in *PARP-1*$^{-/-}$ macrophages, the enzymatic activity of PARP-1 seems to be dispensable for NF-κB–dependent gene expression (17). Finally, consistent with the observation that the activation of caspases can occur rapidly in vivo, e.g., within 2 hours in renal I/R (38), we found that caspase inhibitor Z-VAD-fmk and noncleavable PARP-1 show a protective effect in our I/R models. These findings are reminiscent of previous studies showing that caspase inhibitors attenuate the mouse response to septic

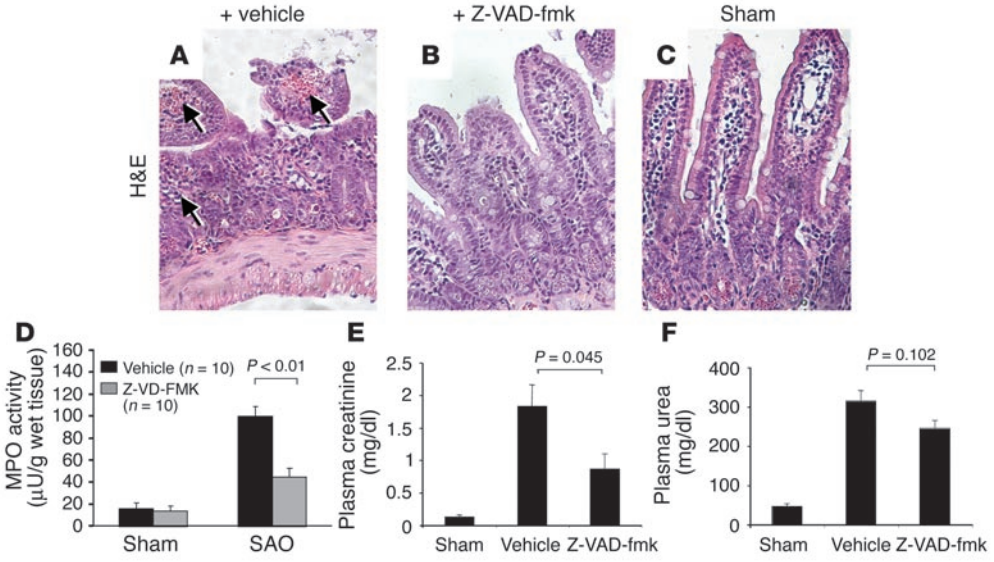

Figure 8
Caspase inhibitor protects mice from I/R treatment. (**A**) The SAO-shocked *PARP-1*$^{+/+}$ ileum pretreated with vehicle exhibiting destroyed mucosa and infiltration of neutrophils and leukocytes (arrows). (**B**) The ileum from a *PARP-1*$^{+/+}$ mouse injected with Z-VAD-fmk prior to SAO treatment showing attenuated damages of villi and mucosa. (**C**) The ileum of a sham-operated animal. Pictures are representative of each group of 10 mice. (**D**) MPO activity in mice treated with caspase inhibitor prior to SAO shock. (**E** and **F**) *PARP-1*$^{+/+}$ mice were subjected to renal I/R with or without a pretreatment with Z-VAD-fmk. The protective effect of the caspase inhibitor against renal dysfunction as shown by urea (**F**) and creatinine (**E**) levels in plasma after renal I/R. Note a reduced production of these markers in Z-VAD-fmk–pretreated animals. Sham: $n = 6$; renal I/R plus vehicle: $n = 4$; renal I/R plus Z-VAD-fmk: $n = 6$. Data in (**D**–**F**) represent the mean ± SEM for n observations.

shock, focal and renal I/R, and allergic airway inflammation in the asthma model (38–43). Although each of these studies has proposed a different mechanism, all of them are linked to the prevention of cell apoptosis. While these mechanisms are plausible, our study provides an additional explanation for their observation on better survivals in caspase inhibitor–treated animals, namely through NF-κB transactivation of cytotoxic molecules. Nevertheless, we cannot absolutely rule out the possibility that Z-VAD-fmk could block the release of cytokines (e.g., IL-1β and IL-18) and thereby protect mice from renal and intestinal I/R (43–45). Taken together, these studies indicate that PARP-1 cleavage may be required for NF-κB transcriptional activity. Since we detected NO only after 24 hours and the PARP-1 cleavage was already visible at 6–12 hours, our study clearly demonstrates that the PARP-1 cleavage is an earlier event than the apoptosis induced by cytotoxic molecules. Although the degree of PARP-1 cleavage was low, it may be significant, given that PARP-1 is abundant in cells, and a small amount of PARP-1 may be sufficient for NF-κB activation. Since PARP-1 fragments can costimulate NF-κB activity (46), it is reasonable to speculate that cleaved fragments of PARP-1 might modulate the interaction of p300 and NF-κB with the basal transcription machinery (46). However, the exact molecular mechanisms have yet to be investigated.

Application of caspase inhibitors has been shown to attenuate intestinal and renal tissue injuries (in our study) and other pathophysiological processes (39–43). The present study, using a genetically engineered mouse model, in which PARP-1 cleavage is abolished, provides novel insights into the significance of caspase cleavage of PARP-1 and highlights the importance of PARP-1 in inflammation and tissue injury. These data demonstrate that repressing caspase activity can prevent PARP-1 cleavage and thereby reduce NF-κB–mediated inflammation response. This information may have strong implications for the development of pharmaceutical strategies to prevent chronic and acute inflammation response.

Methods

Generation of the KI construct and PARP-1$^{KI/KI}$ *mice*. We used a 10-kb *PARP-1* genomic fragment (a kind gift from B. Auer, Institute of Biochemistry, Innsbruck, Austria) containing exons 4–9 to construct a gene targeting vector. A point mutation (GA at nucleotide 640 of the mouse *PARP-1* gene) was introduced into the DEVD box (codons 211–214) as described previously (25). A *neo/tk* cassette flanked by two lox-P sites (a kind gift from E.F. Wagner, Research Institute of Molecular Pathology, Vienna, Austria) was placed in the downstream intron 4. The linearized targeting vector was electroporated into E14.1 ES cells, and targeted ES clones were identified by PCR and Southern blot analyses. To excise the *neo/tk* selection cassette, the targeted ES clones were transfected by a Cre-expressing plasmid, pMC-Cre. After selection in 2 μM ganciclovir (Cymévan; Roche), ES clones containing the D214N mutant (KI) alleles were identified by Southern blotting and injected into blastocysts for production of chimeric mice. Chimeras were crossed with C57BL/6 or 129/Sv animals to generate founder lines. All animal experiments were performed in accordance with the IARC's Animal Care and Use Guidelines.

Isolation of primary cells and culture of cells. MEFs were isolated as described previously (47). Thymocytes were prepared by disruption of the thymus through a 40-μm mesh and were cultured for 24 hours in complete DMEM medium containing 20% FCS. To isolate macrophages, we injected mice 8–10 weeks of age with thioglycollate broth (BD) 3 days prior to the experiment. Peritoneal macrophages were obtained by washing of the peritoneal cavity with a RPMI medium containing 10% FCS and heparin. Primary macrophages and human monocyte/macrophage-like cell line THP-1 were cultured in complete RPMI medium. Primary MLFs were isolated from adult lungs (48) and were cultured in complete DMEM medium. For NO production, macrophages were stimulated with 1 μg/ml LPS, and nitrite was measured using the Griess reagent (49).

Activity assay for PARP-1 and caspase-3. For measurement of PARP-1 activity in vitro, 5×10^5 MEFs were lysed and processed as described previously (47). For measurement of polymer formation in cells by immunofluorescence, DNA damage was induced by 200 μM of H_2O_2 in MEFs. After fixation in 10% trichloroacetic acid, cells were incubated with an anti-PAR antibody (1:200) (LP96-10; Alexis Biochemicals) and Cy-3–conjugated anti-rabbit IgG (DAKO). Cell nuclei were counterstained with DAPI. The caspase activity assay was performed as described previously (21), except that apoptosis was induced by the treatment of thymocytes with 1 μM dexamethasone (Sigma-Aldrich).

Endotoxic shock and measurement of serum cytokines. Mice in a 129/Sv/Ola background were housed in a pathogen-free facility. Sex- and age-matched mice (8–10 weeks of age) were injected intraperitoneally (i.p.) with 30 mg/kg body weight of LPS (0111:B4; Sigma-Aldrich). To measure cytokine production, we collected blood 2 hours after LPS treatment and measured IL-1β and TNF-α concentrations using an ELISA kit (R&D systems). For measuring TNF-α production after intestinal I/R, plasma samples were collected from all animals (n = 10 for each group), and the assay was conducted using a colorimetric commercial kit (Calbiochem-Novabiochem; Merck Biosciences).

Intestinal I/R. Male mice in a 129/Sv/Ola background were anesthetized with urethane (1.3 g/kg body weight, i.p.). Mice (n = 10 for each group) were observed for a 30-minute stabilization period before either splanchnic ischemia or sham ischemia. SAO was induced by clamping both the superior mesenteric artery and the celiac trunk, resulting in a 30-minute occlusion, followed by reperfusion. All the mice were sacrificed at 60 minutes after reperfusion for histological examination and biochemical studies. In another experiment, all the mice were sacrificed at 120 minutes following reperfusion for determination of survival. For caspase inhibitor experiments, mice were injected with 10 mg/kg body weight of Z-VAD-fmk prior to I/R treatments. The vehicle solution consisted of saline containing 1 ml/kg of DMSO.

Renal I/R. Male mice (n = 4–8 for each group) in a 129/Sv/Ola background were anesthetized with avertin (125 mg/kg, i.p.) and subjected to bilateral renal ischemia for 30 minutes, during which the renal arteries and veins were occluded using microaneurysm clamps (37). Microaneurysm clamps were not used on sham-operated mice. After the renal clamps were removed (reperfusion), the mice were observed for 24 hours; blood samples were then collected and mice were sacrificed. Plasma urea and creatinine concentrations were measured as described previously and used as indicators of renal (glomerular) function (37). The plasma levels of AST, an enzyme located in the proximal tubule, were used as an indicator of reperfusion injury (37). Plasma nitrite/nitrate concentrations were examined using the Griess assay (50). For caspase inhibitor experiments, mice were injected with 5 mg/kg body weight of Z-VAD-fmk prior to and 12 hours after the occlusion of the renal arteries and veins. The vehicle solution consisted of saline containing 1 ml/kg of DMSO.

Histological and immunohistochemical analysis. All the histological and immunohistochemistry studies were performed in a double-blinded fashion. After reperfusion, ileum, and kidney tissue biopsies were fixed in a buffered formaldehyde solution as described previously (29). For immunostaining, the sections were incubated overnight with a primary anti-nitrotyrosine antibody (1:1000; Upstate) or with a control including buffer alone or a nonspecific purified rabbit IgG. Immunohistochemistry photographs (n = 5) were assessed by densitometry using Optilab software (Graftek) on a Macintosh computer (CPU G3-266).

MPO activity and determination of MDA levels. Assessment of neutrophil infiltration in the intestine or kidney was performed by measurement of MPO activity, as previously described (51). MPO activity was defined as the quantity of enzyme degrading 1 μmol of peroxide per minute at 37°C and was expressed in microunits per gram of wet tissue. The presence of thiobarbituric acid–reactant substances, an indicator of lipid peroxidation, was determined as previously described (52), in the intestinal tissues. Thiobarbituric acid–reactant substances were calculated by comparison with OD_{650} of standard solutions of 1,1,3,3-tetramethoxypropane malondialdehyde bis(dimethyl acetal) (Sigma-Aldrich) and expressed as MDA levels. The results were analyzed by one-way ANOVA followed by a Bonferroni post-hoc test for multiple comparisons.

Northern blot analysis. Total RNA was prepared from macrophages using Tri-reagent (Sigma-Aldrich). Total RNA (16 μg) was used for Northern blot analysis as described previously (47). Nos-2 cDNA was used as a hybridization probe.

Protein extraction and Western blot analysis. MEFs, thymocytes, and macrophages were lysed for 30 minutes in a hypertonic buffer (20 mM HEPES pH 7.6, 20% glycerol, 500 mM NaCl, 1.5 mM $MgCl_2$, 0.2 mM EDTA, 1 mM DTT, 0.1% NP-40 and protease inhibitors). Human THP-1 cells were treated with 2 μg/ml LPS for the indicated time. Protein samples (25 μg) were resolved on a 10% SDS-PAGE and blotted onto a nitrocellulose membrane (Bio-Rad). Western blots were visualized using the chemiluminescence system (Amersham Biosciences). The following antibodies were used to hybridize blots: anti–PARP-1 (C2-10; R&D Systems); anti–NOS-2 (C-11; Santa Cruz Biotechnology Inc.), anti-actin (C-4; ICN Pharmaceuticals Inc.), and anti-tubulin. Human PARP-1 was detected in THP-1 cell extracts using a human PARP-1–specific polyclonal antibody raised against a baculo-expressed human PARP-1 fragment.

EMSA. Nuclear pellets of macrophages were lysed in a buffer (20 mM HEPES pH 7.6, 25% glycerol, 420 mM NaCl, 1.5 mM $MgCl_2$, 0.1 mM EDTA, 0.1 mM EGTA, 1 mM DTT, 1% NP-40 and 0.5 mM PMSF, 3 μg/ml pepstatin A, 2 μg /ml leupeptin, 40 μM benzamidine). Nuclear extracts (10 μg) were incubated with an end-labeled double-stranded oligonucleotide containing one NF-κB consensus site (5′-GGTTACAAGGGACTTTCCGCTG-3′) in 28 μl of binding buffer (10 mM HEPES pH7.6, 145 mM NaCl, 2.1 mM DTT, 0.8 mM $MgCl_2$, 10% glycerol, 0.05% NP-40, 0.5 μg poly(dI-dC), and 0.35 μg BSA) for 30 minutes. Samples were fractionated on a 5% polyacrylamide gel and visualized by autoradiography.

Transient transfection and NF-κB activity analysis. Primary MLFs at early passages (passages 1–3) were cotransfected with 1 μg pphRSV-nt-βgal reporter construct (46) and 15 μg of *nos-2*(1485/+31WT)-Luc, or of *nos-2*(1485/+31NF-κBmut)-Luc (53). Cells were stimulated with 10 μg LPS or 1,000 U/ml IFN-γ (Sigma-Aldrich) for 12 hours. *PARP-1*$^{-/-}$ peritoneal macrophages were cotransfected with 5 μg of *nos-2*(1485/+31WT)-Luc or of *nos-2*(1485/+31NF-κBmut)-Luc, 1 μg of pphRSV-nt-βgal reporter, together with 5 μg of the PARP-1–expressing vector. The enzyme-dead mutant of PARP-1 (M890V/D899N) was characterized and documented by Rolli et al. (54). These cells were stimulated with 2 μg/ml LPS and 500 U/ml IFN-γ for 12 hours. β-Gal was used as an internal control for transfection efficiency. Luciferase activity was measured as described previously (46).

Acknowledgments

We thank M.-P. Cros for her excellent technical assistance, O. Pluquet for technical advice on EMSA, H. Oshima for technical advice on NO measurement, and M. Perrella (Harvard School of Public Health, Boston, Massachusetts, USA) for providing reagents. We are also grateful to B. Sylla and W.-M. Tong for critical reading and discussion of the manuscript. This study is supported by the Association pour la Recherche sur le Cancer (ARC), France, and the Association for International Cancer Research (AICR), United Kingdom. V. Pétrilli was supported by the Ministry of French Education and by a grant from the ARC. U. Cortes was supported by a fellowship from the International Agency for Research on Cancer (IARC) and by a fellowship from Ligue Nationale contre le Cancer (La Ligue). N.S.A. Patel was supported by a PhD studentship of the William Harvey Research Foundation. P.O. Hassa and M.O. Hottiger are supported by Swiss National Science Foundation grant 31-67771.02 and the Canton of Zurich.

Received for publication April 12, 2004, and accepted in revised form August 3, 2004.

Address correspondence to: Zhao-Qi Wang, International Agency for Research on Cancer (IARC), 150 cours Albert Thomas, 69008 Lyon, France. Phone: 33-4-72-73-85-10; Fax: 33-4-72-73-83-29; E-mail: zqwang@iarc.fr.

1. D'Amours, D., Desnoyers, S., D'Silva, I., and Poirier, G.G. 1999. Poly(ADP-ribosyl)ation reactions in the regulation of nuclear functions. *Biochem. J.* **342**:249–268.
2. Tong, W.M., Cortes, U., and Wang, Z.Q. 2001. Poly(ADP-ribose) polymerase: a guardian angel protecting the genome and suppressing tumorigenesis. *Biochim. Biophys. Acta.* **1552**:27–37.
3. Hassa, P.O., and Hottiger, M.O. 2002. The functional role of poly(ADP-ribose)polymerase 1 as novel coactivator of NF-kappaB in inflammatory disorders. *Cell. Mol. Life Sci.* **59**:1534–1553.
4. Berger, N.A., Sims, J.L., Catino, D.M., and Berger, S.J. 1983. Poly(ADP-ribose) polymerase mediates the suicide response to massive DNA damage: studies in normal and DNA-repair defective cells. *Int. Symp. Princess Takamatsu Cancer Res. Fund.* **13**:219–226.
5. Leist, M., et al. 1997. Apoptosis in the absence of poly-(ADP-ribose) polymerase. *Biochem. Biophys. Res. Commun.* **233**:518–522.
6. Wang, Z.Q., et al. 1997. PARP is important for genomic stability but dispensable in apoptosis. *Genes Dev.* **11**:2347–2358.
7. Burkart, V., et al. 1999. Mice lacking the poly(ADP-ribose) polymerase gene are resistant to pancreatic beta-cell destruction and diabetes development induced by streptozocin. *Nat. Med.* **5**:314–319.
8. Masutani, M., et al. 1999. Poly(ADP-ribose) polymerase gene disruption conferred mice resistant to streptozotocin-induced diabetes. *Proc. Natl. Acad. Sci. U. S. A.* **96**:2301–2304.
9. Oliver, F.J., et al. 1999. Resistance to endotoxic shock as a consequence of defective NF-kappaB activation in poly (ADP-ribose) polymerase-1 deficient mice. *EMBO J.* **18**:4446–4454.
10. Szabo, C., and Dawson, V.L. 1998. Role of poly(ADP-ribose) synthetase in inflammation and ischaemia-reperfusion. *Trends Pharmacol. Sci.* **19**:287–298.
11. Pieper, A.A., Verma, A., Zhang, J., and Snyder, S.H. 1999. Poly (ADP-ribose) polymerase, nitric oxide and cell death. *Trends Pharmacol. Sci.* **20**:171–181.
12. Pieper, A.A., et al. 2000. Myocardial postischemic injury is reduced by polyADPripose polymerase-1 gene disruption. *Mol. Med.* **6**:271–282.
13. Martin, D.R., Lewington, A.J., Hammerman, M.R., and Padanilam, B.J. 2000. Inhibition of poly(ADP-ribose) polymerase attenuates ischemic renal injury in rats. *Am. J. Physiol. Regul. Integr. Comp. Physiol.* **279**:R1834–R1840.
14. Chatterjee, P.K., et al. 2004. 5-Aminoisoquinolinone reduces renal injury and dysfunction caused by experimental ischemia/reperfusion. *Kidney Int.* **65**:499–509.
15. Cohen, J. 2002. The immunopathogenesis of sepsis. *Nature.* **420**:885–891.
16. Kuhnle, S., Nicotera, P., Wendel, A., and Leist, M. 1999. Prevention of endotoxin-induced lethality, but not of liver apoptosis in poly(ADP-ribose) polymerase-deficient mice. *Biochem. Biophys. Res. Commun.* **263**:433–438.
17. Hassa, P.O., Covic, M., Hasan, S., Imhof, R., and Hottiger, M.O. 2001. The enzymatic and DNA binding activity of PARP-1 are not required for NF-kappa B coactivator function. *J. Biol. Chem.* **276**:45588–45597.
18. Hassa, P.O., and Hottiger, M.O. 1999. A role of poly (ADP-ribose) polymerase in NF-kappaB transcriptional activation. *Biol. Chem.* **380**:953–959.
19. Chang, W.J., and Alvarez-Gonzalez, R. 2001. The sequence-specific DNA binding of NF-kappa B is reversibly regulated by the automodification reaction of poly (ADP-ribose) polymerase 1. *J. Biol. Chem.* **276**:47664–47670.
20. Kameoka, M., et al. 2000. Evidence for regulation of NF-kappaB by poly(ADP-ribose) polymerase. *Biochem. J.* **346**:641–649.
21. Herceg, Z., and Wang, Z.Q. 2001. Functions of poly(ADP-ribose) polymerase (PARP) in DNA repair, genomic integrity and cell death. *Mutat. Res.* **477**:97–110.
22. D'Amours, D., Sallmann, F.R., Dixit, V.M., and Poirier, G.G. 2001. Gain-of-function of poly(ADP-ribose) polymerase-1 upon cleavage by apoptotic proteases: implications for apoptosis. *J. Cell Sci.* **114**:3771–3778.
23. Smulson, M.E., et al. 1998. Irreversible binding of poly(ADP)ribose polymerase cleavage product to DNA ends revealed by atomic force microscopy: possible role in apoptosis. *Cancer Res.* **58**:3495–3498.
24. Yung, T.M., and Satoh, M.S. 2001. Functional competition between poly(ADP-ribose) polymerase and its 24-kDa apoptotic fragment in DNA repair and transcription. *J. Biol. Chem.* **276**:11279–11286.
25. Herceg, Z., and Wang, Z.Q. 1999. Failure of poly(ADP-ribose) polymerase cleavage by caspases leads to induction of necrosis and enhanced apoptosis. *Mol. Cell. Biol.* **19**:5124–5133.
26. Boulares, A.H., et al. 1999. Role of poly(ADP-ribose) polymerase (PARP) cleavage in apoptosis. Caspase 3-resistant PARP mutant increases rates of apoptosis in transfected cells. *J. Biol. Chem.* **274**:22932–22940.
27. Los, M., et al. 2002. Activation and caspase-mediated inhibition of PARP: a molecular switch between fibroblast necrosis and apoptosis in death receptor signaling. *Mol. Biol. Cell.* **13**:978–988.
28. Zimmermann, B.J., Arndt, H., Kubes, P., Kurtel, H., and Granger, D.N. 1993. Reperfusion injury in the small intestine. In *Pathophysiology of shock, sepsis, and organ failure.* G. Schlag and H. Redl, editors. Springer-Verlag. Berlin, Germany. 322–335.
29. Cuzzocrea, S., et al. 2002. Role of induced nitric oxide in the initiation of the inflammatory response after postischemic injury. *Shock.* **18**:169–176.
30. Sheridan, A.M., and Bonventre, J.V. 2001. Pathophysiology of ischemic acute renal failure. *Contrib. Nephrol.* **132**:7–21.
31. Paller, M.S. 1994. The cell biology of reperfusion injury in the kidney. *J. Investig. Med.* **42**:632–639.
32. Lieberthal, W., and Levine, J.S. 1996. Mechanisms of apoptosis and its potential role in renal tubular epithelial cell injury. *Am. J. Physiol.* **271**:F477–F488.
33. Weight, S.C., Bell, P.R., and Nicholson, M.L. 1996. Renal ischaemia--reperfusion injury. *Br. J. Surg.* **83**:162–170.
34. Akira, S., Takeda, K., and Kaisho, T. 2001. Toll-like receptors: critical proteins linking innate and acquired immunity. *Nat. Immunol.* **2**:675–680.
35. Guha, M., and Mackman, N. 2001. LPS induction of gene expression in human monocytes. *Cell. Signal.* **13**:85–94.
36. MacMicking, J.D., et al. 1995. Altered responses to bacterial infection and endotoxic shock in mice lacking inducible nitric oxide synthase. *Cell.* **81**:641–650.
37. Chatterjee, P.K., et al. 2003. GW274150, a potent and highly selective inhibitor of iNOS, reduces experimental renal ischemia/reperfusion injury. *Kidney Int.* **63**:853–865.
38. Daemen, M.A., et al. 1999. Inhibition of apoptosis induced by ischemia-reperfusion prevents inflammation. *J. Clin. Invest.* **104**:541–549.
39. Endres, M., et al. 1998. Attenuation of delayed neuronal death after mild focal ischemia in mice by inhibition of the caspase family. *J. Cereb. Blood Flow Metab.* **18**:238–247.
40. Hotchkiss, R.S., et al. 2000. Caspase inhibitors improve survival in sepsis: a critical role of the lymphocyte. *Nat. Immunol.* **1**:496–501.
41. Iwata, A., et al. 2003. A broad-spectrum caspase inhibitor attenuates allergic airway inflammation in murine asthma model. *J. Immunol.* **170**:3386–3391.
42. Neviere, R., Fauvel, H., Chopin, C., Formstecher, P., and Marchetti, P. 2001. Caspase inhibition prevents cardiac dysfunction and heart apoptosis in a rat model of sepsis. *Am. J. Respir. Crit. Care Med.* **163**:218–225.
43. Oberholzer, A., et al. 2000. Differential effect of caspase inhibition on proinflammatory cytokine release in septic patients. *Shock.* **14**:253–257; discussion 257–258.
44. Gracie, J.A., Robertson, S.E., and McInnes, I.B. 2003. Interleukin-18. *J. Leukoc. Biol.* **73**:213–224.
45. Martinon, F., Burns, K., and Tschopp, J. 2002. The inflammasome: a molecular platform triggering activation of inflammatory caspases and processing of proIL-beta. *Mol. Cell.* **10**:417–426.
46. Hassa, P.O., Buerki, C., Lombardi, C., Imhof, R., and Hottiger, M.O. 2003. Transcriptional coactivation of nuclear factor-kappaB-dependent gene expression by p300 is regulated by poly(ADP)-ribose polymerase-1. *J. Biol. Chem.* **278**:45145–45153.
47. Wang, Z.Q., et al. 1995. Mice lacking ADPRT and poly(ADP-ribosyl)ation develop normally but are susceptible to skin disease. *Genes Dev.* **9**:509–520.
48. Bruce, M.C., Honaker, C.E., and Cross, R.J. 1999. Lung fibroblasts undergo apoptosis following alveolarization. *Am. J. Respir. Cell Mol. Biol.* **20**:228–236.
49. Ohshima, H., et al. 1991. L-arginine-dependent formation of N-nitrosamines by the cytosol of macrophages activated with lipopolysaccharide and interferon-gamma. *Carcinogenesis.* **12**:1217–1220.
50. Millar, C.G., and Thiemermann, C. 1997. Intrarenal haemodynamics and renal dysfunction in endotoxaemia: effects of nitric oxide synthase inhibition. *Br. J. Pharmacol.* **121**:1824–1830.
51. Mullane, K.M., Kraemer, R., and Smith, B. 1985. Myeloperoxidase activity as a quantitative assessment of neutrophil infiltration into ischemic myocardium. *J. Pharmacol. Methods.* **14**:157–167.
52. Ohkawa, H., Ohishi, N., and Yagi, K. 1979. Assay for lipid peroxides in animal tissues by thiobarbituric acid reaction. *Anal. Biochem.* **95**:351–358.
53. Perrella, M.A., et al. 1999. High mobility group-I(Y) protein facilitates nuclear factor-kappaB binding and transactivation of the inducible nitric-oxide synthase promoter/enhancer. *J. Biol. Chem.* **274**:9045–9052.
54. Rolli, V., O'Farrell, M., Menissier-de Murcia, J., and de Murcia, G. 1997. Random mutagenesis of the poly(ADP-ribose) polymerase catalytic domain reveals amino acids involved in polymer branching. *Biochemistry.* **36**:12147–12154.